III. Preparation Procedures for Specific Iron Hydroxide and Oxide Compounds

III.A. "Amorphous" Precipitate - Ferrihydrite

When ferric solutions are rapidly hydrolyzed in the laboratory brown colloidal precipitates are formed and often they are referred to as "iron-oxide-hydrate gels", "ferric hydroxide", "hydrous ferric oxide", or "brown amorphous ferric hydroxide" (III.1). These materials are poorly crystalline or amorphous and of ill-defined composition depending on synthesis methods. X-ray diffraction patterns were first obtained by Van der Giessen (III.2), and independently by Towe and Bradley (III.3), for products precipitated from trivalent iron nitrate solutions. Chukhrov et al. (III.4) presented detailed diffraction, infrared absorption, and other data for a natural ferric hydroxide from the URSS. They proposed ferrihydrite as a new name for a ferric hydroxide of formula which they considered to be $Fe_5(O_4H_3)_3$ and showing five X-ray diffraction lines indicative of a defect hematite structure as suggested by Towe and Bradley (III.3) who proposed the formula $Fe_5HO_8 \cdot 4H_2O$. Russell (III.5) has shown that when adsorbed water is carefully removed, OH absorption bands can be detected by IR spectroscopy and has suggested that the formula should be amended to $Fe_2O_3FeOOH \cdot 2.6H_2O$, or $FeOOH \cdot 0.5H_2O$ which agrees very well with that proposed by Van der Giessen (III.2), $FeOOH \cdot 0.3H_2O$.

The morphology of such poorly crystalline preparations consists of "minute particles of about 30 A in diameter" (III.2), or "extremely fine particles with average dimensions less than 50 A" (III.3). For a natural material Schwertmann and Fisher (III.6) found rounded aggregates several tenths of a micrometer in diameter which

seem to consist of small discrete particles approximately 100 A in diameter. However, they calculated from XRD data a mean radius of spherical particles of 50 A for synthetic products.

Cornejo et al. (III.1) made a study to compare two ferrihydrate samples prepared by different methods; they employed X-ray powder diffraction (XRD), infrared spectroscopy (IR), transmission electron microscopy (TEM), and nitrogen adsorption techniques. The method of preparation of sample 1 was similar to that used by Towe and Bradley (III.3). A 0.06 M solution (freshly prepared) of $Fe(NO_3)_3 \cdot 9H_2O$ was hydrolyzed by heating to 85°C. The resulting sol was dialyzed against distilled water until nitrate-free. An aliquot of this suspension was removed for examination by electron microscopy. The remainder was dried at 50 and/or 110°C for other studies. Sample 2 was obtained by the method of Russell (III.5) by boiling a 0.01 M aqueous solution of $Fe(NO_3)_3 \cdot 9H_2O$ to effect precipitation, and then dialyzing it against distilled water. The product was isolated by freeze-drying.

XRD analysis showed peaks at 2.52, 2.24, 1.97, 1.51 and 1.47 A for sample 1 and 2.53, 2.25, 1.97, 1.51 and 1.47 A for sample 2. These data matched closely those reported by Towe and Bradley (III.3) and Russell (III.5) for their synthetic ferrihydrites. Both samples show the reflexion (113) at 1.97 A, characteristic of ferrihydrite (III.4). No evidence of more crystalline oxides or oxyhydroxides was detected in XRD or IR spectra, and no differences between samples 1 and 2 were observed.

Adsorption isotherms of nitrogen on the two samples at 77°K are different. That of sample 1 (Figure III.1a) belongs to type IV of the BDDT (III.7) classification

with marked hysteresis on desorption to a relative pressure of 0.35. The shape of the hysteresis loop has characteristics like those described as type A and B by de Boer (III.8). On the other hand the sample 2 belongs to type II and exhibits an hysteresis loop less marked than sample 1 (Figure III.1b), and its shape could be described as type A.

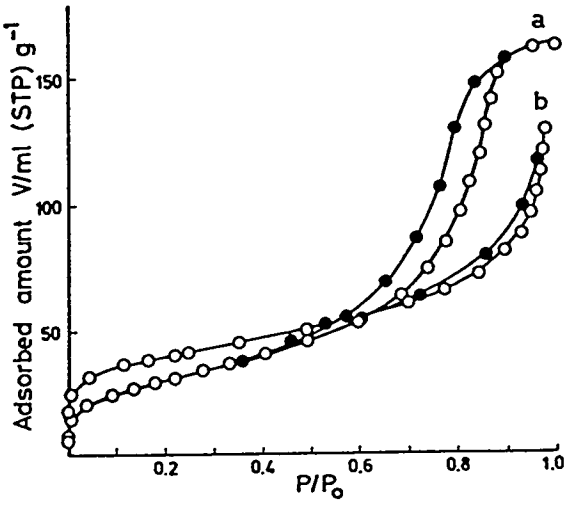

Figure III.1. Nitrogen adsorption isotherms at 77K of samples 1 (a) and 2 (b) [from reference III.1].

t-Plots are given in Figures III.2a and b. In both cases a straight line passing through the origin is obtained at low relative pressures. For sample 1 a considerable upward deviation at t > 0.5 nm is observed showing the absence of microporosity and then the t-plot becomes horizontal at t > 1.3 nm (Figure III.2a). This indicates enhanced adsorption due to capillary condensation of nitrogen in mesopores and in the region of contact between particles. Therefore the area available for further adsorption is considerably reduced, so that the t-plot becomes almost horizontal. On the other hand the t-plot corresponding to sample 2 shows a continuous downward deviation indicating the presence of micropores (radius < 2.0 nm). Although the t-plot for this sample indicates only micropores, the authors state that the hysteresis effect observed

in the nitrogen adsorption-desorption isotherm (Figure III.1b) is characteristic of materials containing pores of intermediate sizes. Actually, the isotherm observed for sample 2 (III.1b) is what is expected for a material composed of nonporous, spherical particles such as Cab-o-Sil or Degussa alumina oxide C; thus, we believe this material is essentially "nonporous".

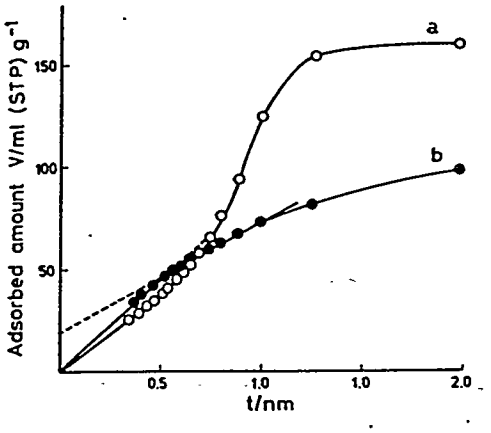

Figure III.2. t-Plots corresponding to the nitrogen isotherm at 77K of Figure III.1 [from reference III.1].

It is found that in both samples the total surface area, S_t, obtained by the t-method, is in good agreement with the BET specific surface area, S_{BET} (Table III.1), suggesting that both the t and BET methods give a consistent surface area for these two samples. Cumulative surface areas, S_{cum}, in the mesopore range are included in Table III.1. The agreement is worse in the case of sample 2 because mircopores are not taken into account in the computation presented in Table III.1. The results show that sample 1 contains slit-shaped mesopores according to the de Boer model (III.8) whereas sample 2 seems to be composed by cylindrical mesopores according to Dollimore and Heal (III.9). Again, we disagree with the authors conclusions; sample 1 appears to have cylindrical pores and sample 2 appears to be "nonporous".

Table III.1

Results from N_2 Adsorption at 77°K

		m^2g^{-1}		
Sample	C	S_{BET}	S_t	S_{cum}
1	85	109.0	113.0	112.0
2	59	137.0	140.0	61.7

TEM micrographs obtained for sample 2 are very similar to those shown by other workers (III.2, III.3) for similar synthetic materials. However, sample 1 micrographs present an external habit different from that of sample 2. The morphology of sample 1 is rather similar to that shown by Fisher and Schwertmann (III.10) for a poorly crystallized hematite obtained from amorphous iron hydroxide. In both cases a granular internal structure and a very poorly developed hexagaonal shape are visible indicating a generic relationship between ferrihydrite and hematite. It seems that a well-crystallized ferrihydrite has a morphology similar to a poorly crystallized hematite when both samples are derived from amorphous iron hydroxides. This fact could suggest that hematite crystallizes within ferrihydrite aggregates by internal rearrangement and dehydration according to the conclusions of Fisher and Schwertmann (III.10).

III.B. α-FeOOH - Geothite

The early stages in the precipitation of the thermodynamically stable solid phase (geothite) from acidified iron(III) solutions has been followed at 25°C (III.11) and in the temperature range 25-95°C (III.12). Within a period of one day at 25°C the

formation of a colloidal solution of amorphous iron(III) hydroxide particles of quite uniform size (5 nm) was complete. The kinetics of nucleation and of the growth of the dispersed phase that serves as a precursor for the formation of geothite was observed to depend upon the parameter α_o = $(OH/Fe)_o$. By assuming growth of a constant number of critical nuclei, the experimental results were separable in time to a proper growth stage and a stage of mixed nucleation and growth.

Acidified solutions of 0.1M $Fe(NO_3)_3$ and ionic strength of 0.89M were titrated with 2.5M NaOH using either: (1) a constant rate of addition of base or (2) or constant pH maintained by base addition. The precipitate formed at the end of the experiment was aged for a period of 2 or 3 days at the titration temperature for values of pH 7 and 10.

Simple titration of iron solutions with NaOH was illuminating. The data in Figure III.3 is illustrative. The characteristic feature of these curves is the plateau region

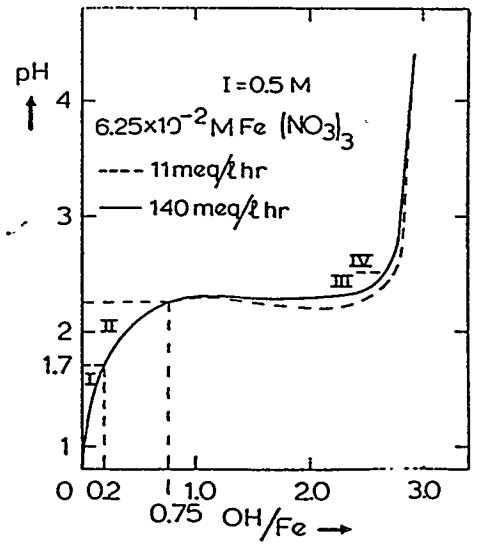

Figure III.3. Typical base titration curves (pH versus OH/Fe) at two titration rates. The four different regions are indicated (see text for detail) (from reference III.11).

(III.13) where the major change in [OH]/[Fe] occur. By interrupting the titration at various points along the curve in Figure III.3 and allowing the pH to change without further additions, the curve was divided into four regions (labeled I, II, III, and IV in Figure III.3). Solutions with OH/Fe values in region I undergo no change with time even though they are supersaturated with respect to the thermodynamically stable phase, geothite. Thus, this region corresponds to the formation of soluble hydrolysis products ($FeOH^{2+}$, $Fe(OH)_2^{+}$, $Fe_2(OH)_2^{4+}$, etc.); the formation of these species is much faster than the fastest titration speed utilized in this study. Species present in region II do "relax" to produce a gradual lowering of the pH, and eventually a solid phase forms. The relaxation always includes an induction period during which the pH does not change even though color changes indicates that higher polymeric species are being formed. In region II there is not an induction period. Depending upon titration speed, a pH is attained where a plateau is attained (region (III)); in Figure III.3 this is at pH about 2.4 where formation of the solid phase is essentially complete. In region IV neutralization of the remaining acid and the positive surface charge of the colloidal particles are the alkali-consuming processes. Increasing the ionic strength results in a decrease in, and a gradual disappearance, of region II.

As shown in Figure III.4, curve B, obtained at a lower pH than for curve A, exhibits a measurable lag in time prior to "relaxing". From a number of curves like B, the authors obtained characteristic induction times, t_i, as illustrated in Figure III.4. This parameter is located by the intersection of the tangent to the point of maximum base addition with the time axis, as was done by Dousma and de Bruyn (III.13). Plots of t_i vs. pH (or pFe_t) are illustrated in Figure III.5 and show that t_i changes from near

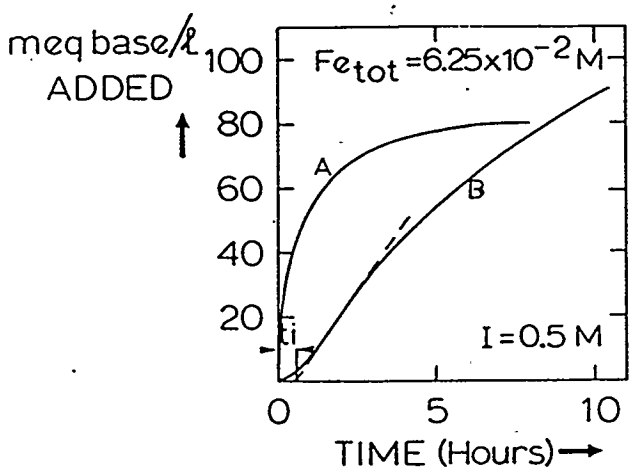

Figure III.4. **Typical relaxation curves. Curve A: pH = 2.28, α_o = 0.46. Curve B: pH = 2.10, α_o = 0.21 (from reference III.11).**

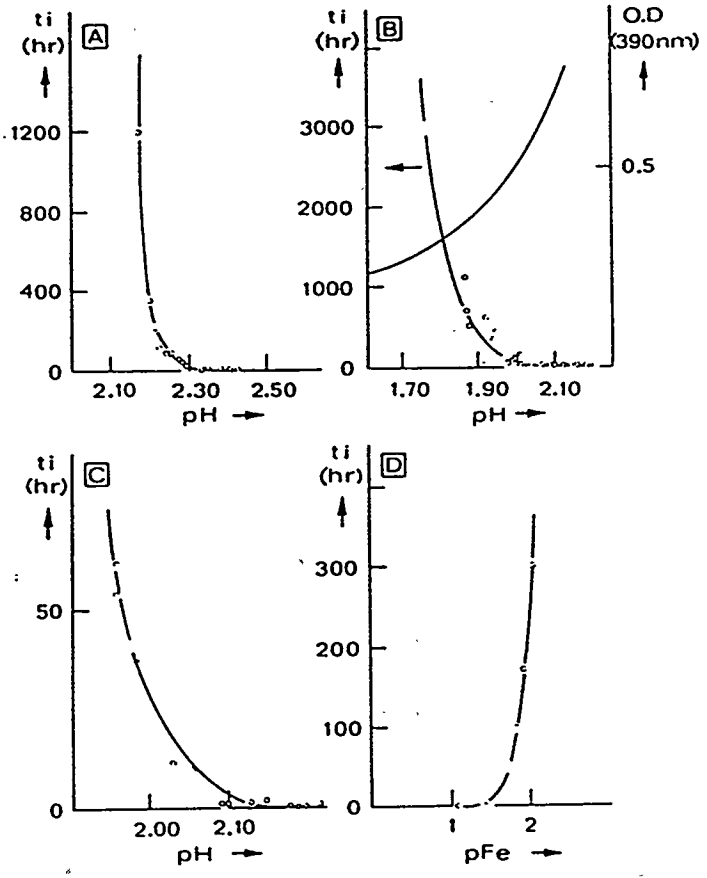

Figure III.5. **Induction periods, t_i, as a function of pH and pFe(III). A. Total iron(III) nitrate concentration 6.25 x 10^{-3} M. Initial ionic strength 0.1 M. B. Total iron(III) nitrate concentration 6.25 x 10^{-2}M. The change of the optical density (OD) with pH is illustrated. Type A experiment. C. Same as B except for enlarged ordinate axis. D. pH 2.11, total ionic strength 1.0 M $NaNO_3$ (from reference III.11).**

zero to nearly ∞ over a narrow pH range (at most 0.5 pH units). Following the procedure of Feenstra and de Bruyn (III.4), two precipitation boundaries can be located for this system. Be extrapolation of ($t_i \rightarrow \infty$) a lower limiting pH (or pFe_t) is found which locates the boundary separating region I from region II in Figure III.3. The boundary separating regions II and III is located by the pH (or pFe_t) value for which $t_i < 1$ min. A plot of *ln* t_i versus ΔpH (ΔpH = pH - pH ($t_i \rightarrow \infty$)) results in three parallel straight lines for each of the ions used in the study (Figure III.6). The change

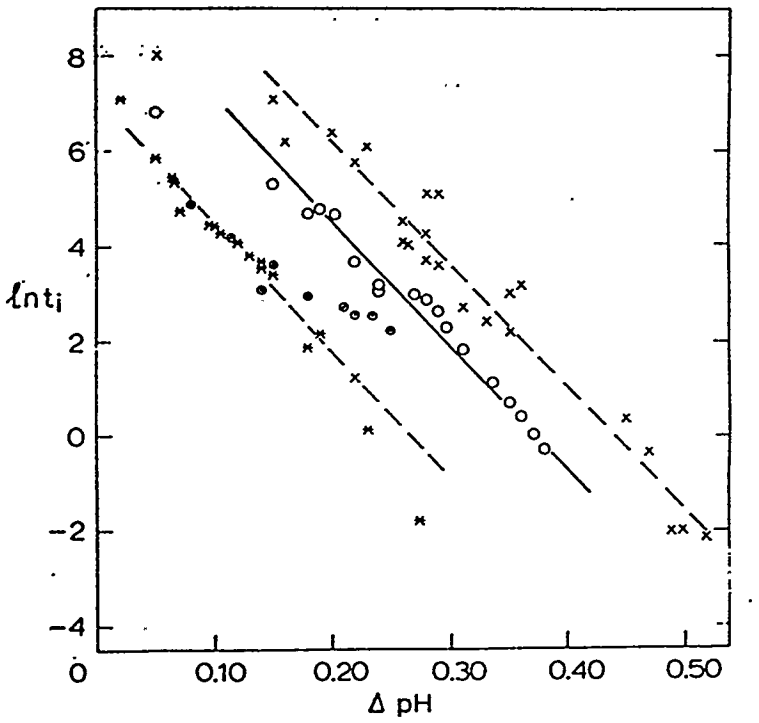

Figure III.6. **The logarithm of measured induction time versus ΔpH, ΔpH = pH(t_i) - pH($t_i \rightarrow \infty$). Total iron(III) perchlorate concentration 4 x 10^{-2}M. Total iron(III) chloride concentration 6.25 x 10^{-3} M. x Total iron(III) nitrate concentration 6.25 x 10^{-2} M (from reference III.11).**

in *ln* t_i with ΔpH largely depends upon the nature of the anion and the total iron(III) concentration. This produced an empirical relation between t_i and $[H^+]$:

$$t_i = B[H^+]^{14\pm1} \qquad \text{[III.1]}$$

where B is a constant at a fixed total Fe(III) concentration and for a specified counter ion.

The parameter α(t), obtained by dividing the total amount of alkali added to a fixed amount of Fe(III) by the total alkali needed to precipitate geothite, is approximately

$$\alpha(t) = OH(t)/3Fe. \qquad \text{[III.2]}$$

Typical growth curves (α vs. t) are given in Figures III.7 and III.8. The relaxation rate ($d\alpha/dt$) varies considerably within a small pH interval (ca. 0.2 pH unit). The shape of

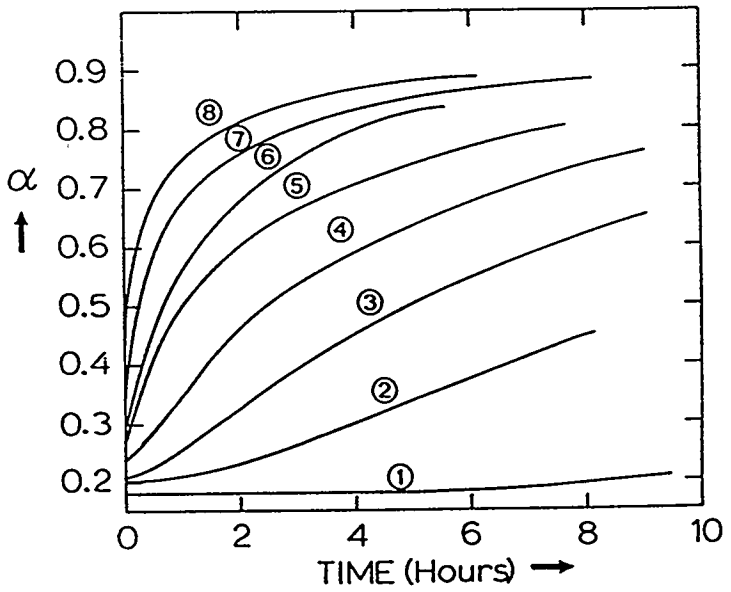

Figure III.7. **Typical examples of growth curves (α versus t). I = 0.5 M. Curves 1 and 3-8 refer to total iron(III) nitrate concentration 6.25 x 10^{-2} M, curve 2 to total iron(III) nitrate concentration 1.56 x 10^{-2} M and curve 6 to total iron(III) concentration 3.12 x 10^{-3} M. 1. pH 2.04. 2. pH 2.28. 3. pH 2.10. 4. pH 2.15. 5. pH 2.20. 6. Fe(III) = 6.25 x 10^{-2} M, pH 2.22; Fe(III) = 3.12 x 10^{-2} M, pH 2.28. 7. pH 2.25. 8. pH 2.28 (from reference III.11).**

the curve is controlled by the value of α_o and an induction period is observed for low α_o values (Figure III.7). An S-shaped curve is observed for intermediate α_o values but at higher α_o values an induction period is not noted. All curves approach asymptotically the $\alpha = 1$ level. A comparison of the curves in Figures III.7 and III.8 show that the shape of the curve is determined largely by α_o.

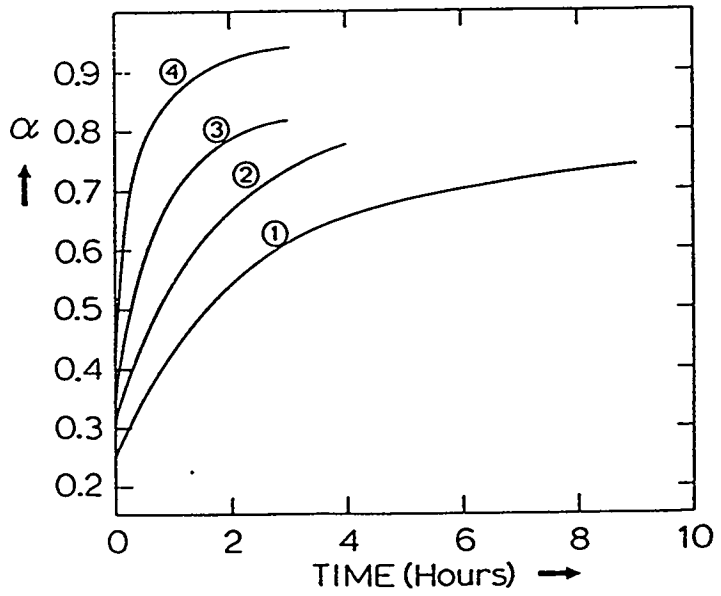

Figure III.8. Typical examples of growth curves (α versus t) for total iron(III) nitrate concentration 6.25 x 10^{-2} M and I = 1.0 M. 1. pH 2.12. 2. pH 2.15. 3. pH 2.18. 4. pH 2.24 (from reference III.11).

The available thermodynamic information for the system is summarized in Figure III.9. The straight line A locates the composition of solutions in equilibrium with geothite at room temperatures. Straight line B is a plot of the relation $\log A_{Fe^{3+}} - 3 \log a_{OH^-} = pFe^{+3} + 3\ pOH^- = 38.7 \pm 0.1$ and gives the composition of the solutions which, although clearly supersaturated with respect to geothite, are on the threshold of decomposing to the amorphous solid phase. Line B was evaluated

from the experimental induction time measurements and describes the lower limit of metastable solutions. Curve C was calculated taking into account iron hydroxo-complexes such as $Fe(OH)^{2+}$, $Fe_3(OH)_4^{5+}$, etc. (see original reference for calculation details). Curve C forms the upper kinetic boundary of metastable solutions.

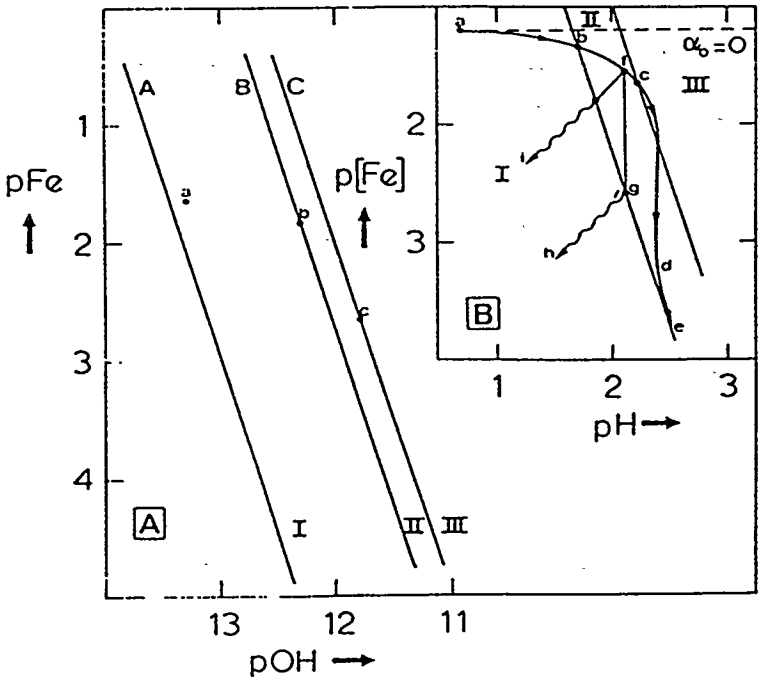

Figure III.9. Precipitation diagram. Boundary A represents the saturation line for α-FeOOH with an assumed activity solubility product $10^{-41.0}$. Boundary B represents the saturation line for the amorphous precursor (activity solubility product $10^{-38.23}$). Curve C locates the approximate kinetic boundary for spontaneous precipitation. I, II and III refer to the stages in Figure III.3. B. The experimental paths followed during the base titration of an acidified 6.25 x 10^{-2} M iron(III) solution. For details see text (from reference III.11).

The degree of supersaturation π, which plays a role in determining the rate of formation and growth of the precursor amorphous phase from the metastable phase in region II (Figure III.9), is

$$\pi = IP/Ksp \qquad \text{[III.3]}$$

where IP is the ionic activity product $A_{Fe^{3+}}(A_{OH^-})^3$ in region II and ksp = $10^{-38.7\pm0.1}$ is the solubility product of the precursor phase.

Various allowed experimental pathways are diagrammed in the inset of Figure III.9. Curve a b c d e traces the path followed during a typical titration experiment starting with the "undersaturated" solution of pH 0.7. Up to a point inside region II this curve describes equilibrium changes. The curve f i describes the general behavior during a free relaxation experiment. Curve f g h sketches approximately the path followed during a constant pH relaxation through the metastable region (up to point g) followed by a further free relaxation. The time consumed at 25°C in moving from f to g is of the order of hours whereas the free relaxation in the region (g h) that results in the transformation of the amorphous precursor to geothite extends over months.

Two important observations were made in these studies: (1) long induction periods may be observed where pH remains essentially constant and (2) the final size of the colloidal particles (determined by electron microscopic examination) is relatively independent of pH and the particular relaxation method. A quite monodisperse material is obtained with an average particle diameter between 3 and 5 nm.

Whereas in the early stages of the relaxation studies nucleation may play a role, it is to be expected that growth of the amorphous precursor to its eventual maximum average size of about 5 nm is the major kinetic process. Assuming growth of a constant number of uniformly sized particles, an expression for the linear growth rate

of the precursor can be derived. At constant pH the removal of iron(III) from the solution by the growing particle may be expressed by

$$- \frac{dC(t)}{dt} = k_r C(t)^m O(t) \qquad \text{[III.4]}$$

where C(t) represents the total concentration of soluble iron(III) in the solution at time **t**; O is the total area of the growing particles exposed to the solution at time **t**; $\mathbf{k_r}$ is a pseudo-reaction rate constant and **m** a constant defining a so-called "order" of the reaction with respect to soluble iron(III). Assuming that the particles grow as spheres with an average radius < r(t) >, a mass balance shows

$$C_o - C(t) = \frac{N}{V_s} \frac{4\pi}{3} <r(t)>^3 \qquad \text{[III.5]}$$

where N is the number of growing particles per unit volume of solution, V_s, the molar volume of the solid, and C_o the total initial concentration of soluble iron(III). The linear growth rate

$$r = d <r(t)> /dt = k_r V_s C(t)^m \qquad \text{[III.6]}$$

and the time rate of change of total soluble iron(III)

$$- \frac{dC(t)}{dt} = k_r (36\pi N V_s^2)^{1/3} (C_o - C(t))^{2/3} C(t)^m \qquad \text{[III.7]}$$

are obtained by combining Equations (III.4) and (III.5). The degree of reaction α(t) introduced in plotting the relaxation curves (Figures III.7 and III.8) may be approximated by the expression

$$\alpha(t) = \frac{C_o - C(t)}{C_o - C_e} \qquad \text{[III.8]}$$

where C_e is the equilibrium iron(III) concentration which is practically zero. With the aid of Equation [III.8], Equation [III.7] may be transformed to yield

$$\frac{d\alpha}{dt} = k_m(1-\alpha)^m\alpha^{2/3} \qquad \text{[III.9]}$$

where

$$k_m = k_r(36\pi N V_s^2)^{1/3}(C_o - C_e)^{(m-1/3)} \qquad \text{[III.10]}$$

Equation [III.9] predicts an S shaped growth curve (α versus t) with the inflection point at

$$\alpha = 2/(3m + 2) \qquad \text{[III.11]}$$

Equation [III.9] has the same form as that derived by Nielsen (III.15) for a polynuclear growth model. It also resembles an expression derived by Makrides et al. (III.16) for the initial stages in the growth of amorphous silica.

On taking the logarithm of Eq. [III.9] and rearranging terms,

$$\log\left(\alpha^{-2/3}\,\frac{d\alpha}{dt}\right) = \log k_m + m\,\log\,(1-\alpha) \qquad \text{[III.12]}$$

This equation allows one to evaluate graphically the magnitude of the exponent **m** and the dependence of $\mathbf{k_m}$ on the pH. The application of Eq. [III.12] in the analysis of the experimental α-t curves is subject to certain restrictions: (a) nucleation is essentially completed in the early stages of the relaxation process, (b) Ostwald ripening does not

occur in later stages, and (c) a phase transformation (amorphous → crystalline geothite) does not take place. The rather uniform size of particles in the end product which remain amorphous confirms that restriction (c) is not violated and that nucleation must be restricted to the early stages of the relaxation process. The small size of the final product may be cited as evidence in favor of restriction (b).

Typical examples of the applicability of Eq. [III.12] to the experimental relaxation results are given in Figure III.10. The linear relation predicted by Eq. [III.12] is seen to be obeyed quite well, especially for those experiments in which α_o exceeds a value of 0.35. A value of m = 3.1 $\pm$ 0.4 (equal to the slope of the straight line) is obtained, independent of ionic strength, total iron(III) concentration and α_o (or pH_o). When $\alpha_o \leq 0.35$, a straight line with slope m = 3.1 is only obtained after the plotted curve passes through a minimum at an α value of 0.33 $\pm$ 0.02 regardless of

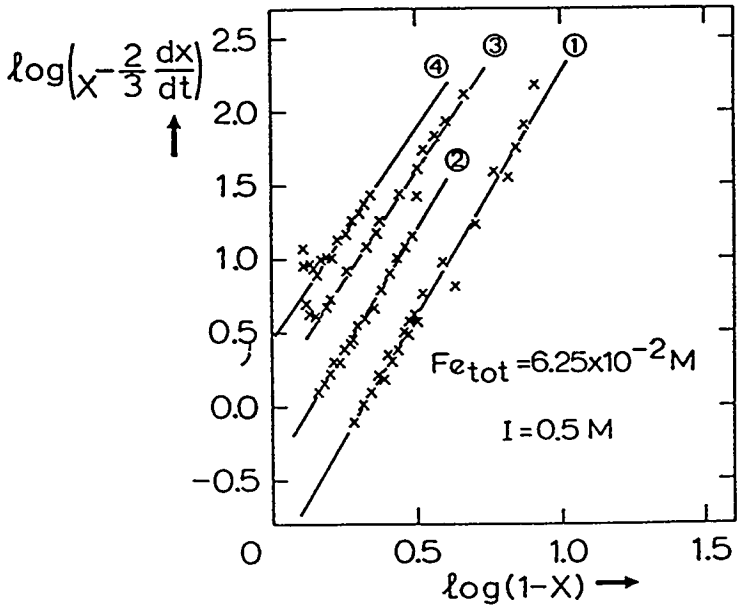

Figure III.10. Analysis of the growth curves of solutions with total iron(III) concentration 6.25 x 10^{-2} M and I = 0.5 with the aid of Eq. [III.12]. 1. α_o = 0.46; pH 2.28. 2. α_o = 0.29; pH 2.22. 3. α_o = 0.24; pH 2.15. 4. α_o = 0.21; pH 2.10 [from reference III.11].

the particular α_o value. This inflection point in the experimental α versus t curve however falls higher than that predicted (α = 0.18) by theory (Eq. [III.11]).

The location of the inflection point in the experimental α-t curves (Figures III.7 and III.8) may therefore be regarded as a measure of the duration of the nucleation stage. In Figure III.11 plots of log k_m versus pH are shown, where log k_m is the intercept on the ordinate axis in Figure III.10. Parallel straight lines are obtained with a slope $N_{OH} = 7.5 \pm 1$ independent of ionic strength.

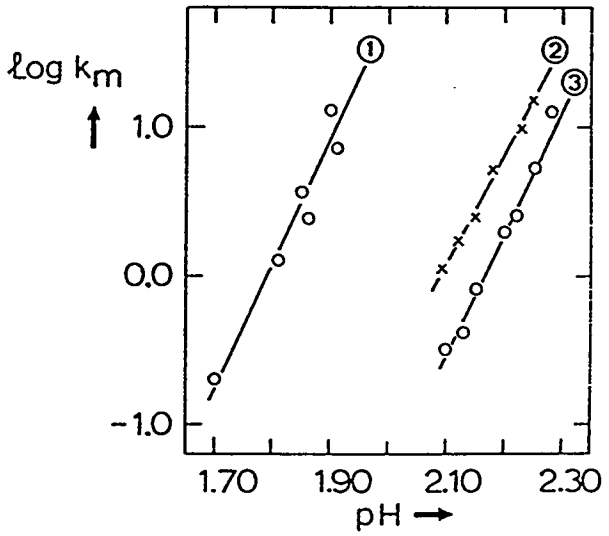

Figure III.11 **Plots of log k_m versus pH at three ionic strengths. 1. I = 3.0 M. 2. I = 1.0 M. 3. I = 0.5 M [from reference III.11].**

The exponent m, empirically introduced in Eq. [III.4], may now be given some physical significance. The growth of the amorphous phase will involve transfer of an iron(III)-bearing solute, $Fe_x(OH)_y^{(3x-y)+}$, the so-called growth unit, from the solution to the solid surface where it will react and be incorporated into the solid lattice. This process may be represented by the overall reaction

$$Fe_x(OH)_y^{(3x-y)+} + (3x-y)H_2O \rightarrow xFe(OH)_3 + (3x-y)H^+ \qquad \text{[III.13]}$$

The concentration of this "growth unit" will then be related to that of the total amount of dissolved iron, C(t) raised to the power m. Insufficient information about the composition of the solution during growth unfortunately does not justify the authors to make further speculation about the exact nature of this growth unit.

Van der Woude and de Bruyn (III.11) comment briefly on the relative constant size of the colloidal product independent of the experimental conditions, an observation also made by other investigators (III.17 - III.19). Buyanov et al. (III.18) suggested that the uniform final particle size is about equal to that of the critical nucleus, in other words growth hardly takes place. Sommer et al. (III.20) assumed that the limited particle size is due to simultaneous occurrence of structural changes and growth, which should be competitive. Van der Woude and de Bruyn (III.11) believe that their observations argue against the validity of the explanations put forward by these earlier investigators. They believe that particles of uniform size may be expected when the rate of nucleation depends in an identical way on pH (or α_o) as does the rate of growth, for instance, via the concentration of the same iron(III)-bearing solute species. They believe that this may be the case in the formation of an iron(III) hydroxide dispersion and that this is supported by the observed invariance of the location of the inflection point in the experimental α-t curves (at $\alpha = 0.33 \pm 0.02$).

Van der Woude et al. (III.12) carried out similar studies at higher temperatures. Results of precipitation and aging studies conducted at pH 7 or 10 and over the temperature range 25-95°C are summarized in Table III.2. Crystal phases were

Table III.2
Characteristics of Aged Precipitate (aging time 2-3 days) at pH 7 and 10 Produced by Homogeneous Titration (from reference III.12)

	pH = 7			pH = 10	
Temp. (°C)	IR	X-ray	BET (m^2/g)*	IR	X-ray
25	amorphous	amorphous	301	amorph/α-FeOOH	amorphous
35	amorphous	amorphous	276	amorph/α-FeOOH	amorphous
45	amorphous	amorphous	263	α-FeOOH	amorphous
55	amorphous	amorphous	235	α-FeOOH	α-FeOOH
65	amorphous	amorphous	224	α-FeOOH	α-FeOOH
75	amorphous	amorphous	177	α-FeOOH/α-Fe_2O_3	α-FeOOH/α-Fe_2O_3
85	amorph/α-Fe_2O_3	amorph/α-Fe_2O_3	156	α-FeOOH/α-Fe_2O_3	α-FeOOH/α-Fe_2O_3
95	amorph/α-Fe_2O_3	amorph/α-Fe_2O_3	135	α-FeOOH/α-Fe_2O_3	α-FeOOH/α-Fe_2O_3

* Measurement accuracy 5%

identified by infrared (IR) spectra and XRD. These data clearly show that it is possible to prepare essentially pure α-FeOOH under the proper conditions. The pH also plays a critical role since, except at very high temperatures, an amorphous material is obtained at pH 7 but a crystalline material results at a pH of 10. For the pH 7 precipitation, there is a continuous decrease in surface area with an increase in precipitation - aging temperature (Figure III.12).

Van der Woude et al. (III.12) chose to compare results in two temperature ranges: 25 to about 70°C and 85 to 95°C. The curves at 55°C (Figure III.13) are similar to others in the 25 to 70°C temperature range (compare Figures III.7 and III.8). For these curves the shape is largely determined by the size of α_o. The influence of temperature at a constant $\alpha_o = 0.25$ is illustrated in Figure III.14; the data show that the initial rate of relaxation ($d\alpha/dt$, equation [III.12]) increased rapidly with

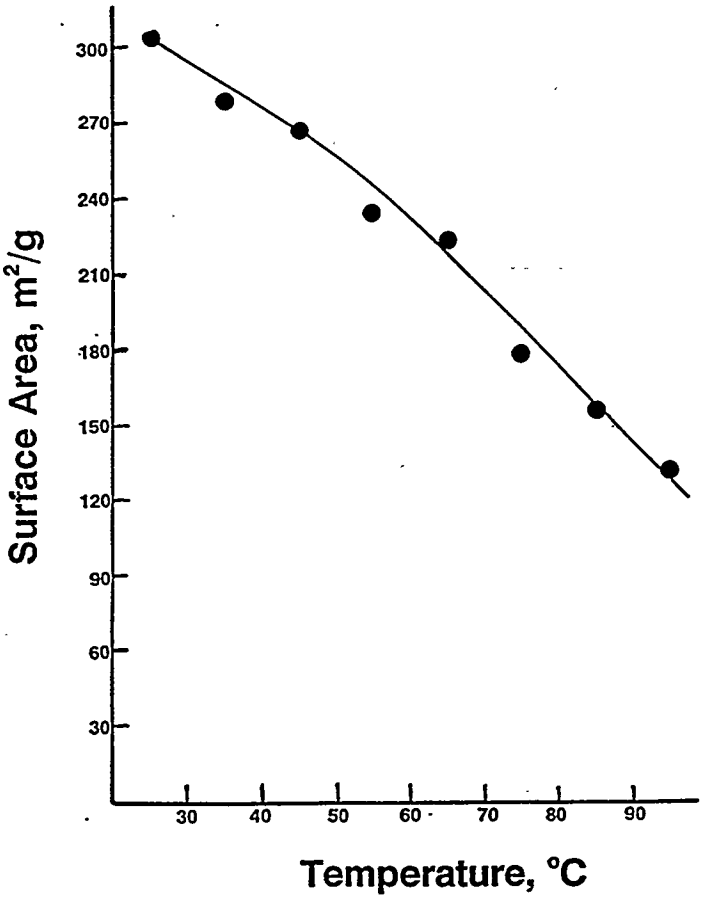

Figure III.12. Surface area from reference III.12 of aged precipitates with increasing aging temperatures.

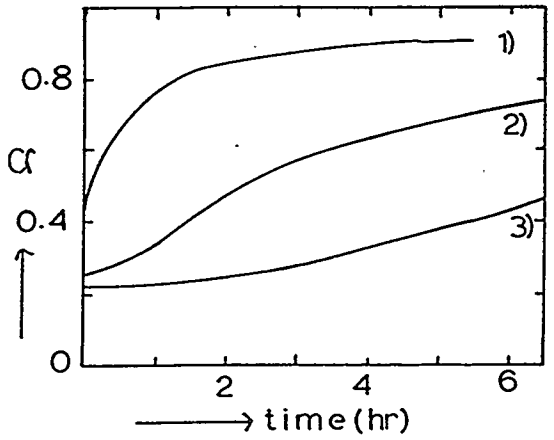

Figure III.13. Relaxation curves (α versus time) at 55°C at different α_o values. For definition of α and α_o see text. 1. α_o = 0.42, pH 1.59. 2. α_o = 0.25, pH 1.46. 3. α_o = 0.22, pH 1.38 (from reference III.12).

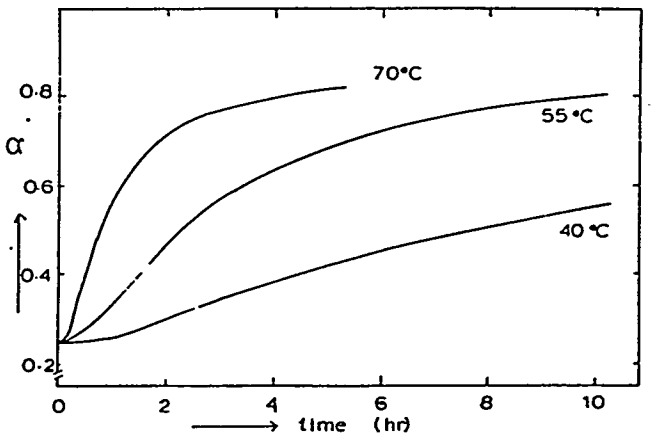

Figure III.14. Relaxation curves at different temperatures, but constant α_o = 0.25 (from reference III.12).

increasing temperature. Induction times, calculated using equation [III.1] with an exponent of 13, rather than 14, for various pH and temperatures are summarized in Table III.3. These data suggest that an induction period is a factor only at the very

Table III.3

Induction Times Obtained from the Growth Curves According to Eq. [III.1] at Various pH Values and Temperatures (from reference III.11)

25°C		40°C		55°C		70°C	
pH (α_o)	t_i (min)	pH (α_o)	t_i (min)	pH (α_o)	t_i (min)	pH (α_o)	t_i (min)
1.80(0.17)	*	1.69(0.18)	**	1.35(0.18)	280	1.11(0.19)	31
1.90(0.25)	156	1.71(0.22)	120	1.38(0.22)	55	1.17(0.25)	12
1.98(0.28)	60	1.72(0.25)	58	1.46(0.25)	18	1.25(0.32)	~1
2.03(0.32)	18	1.75(0.29)	25	1.51(0.32)	~3	1.28(0.41)	0
2.07(0.37)	6	1.77(0.32)	10	1.54(0.33)	< 1		
		1.83(0.37)	~2	1.59(0.42)	0		
m = 3.3		m = 3.2		m = 3.0		m = 2.8	

* >>3 days; ** 20 hr.

low pH regions (less than pH = 3). Over the temperature range the "reaction order" **m** in the total amount of soluble iron(III) at time **t** is found to be equal to 3.1 $\pm$ 0.4. The value of N_{OH} = d log k_m/dpH is 8 $\pm$ 2 although k_m, the psuedo reaction rate constant at constant pH, increases with temperature at fixed α.

A comparison of the relaxation behavior of solutions at temperatures above 75°C with that in the lower temperature range revealed some striking differences in the physical appearance of the relaxing systems, and in the dependence of the shape of the relaxation curves when $\alpha_o \leq 0.13$, an orange-red precipitate forms in contrast with a clear colorless supernatant. This orange-red precipitate is characteristic of the solid, hematite. At higher α_o values the supernatant becomes increasingly dark brown in color, which is typical of the amorphous colloidal phase observed at lower temperatures. Ultra-centrifugal studies of these relaxing systems indicate that at $\alpha_o <$ 0.13 two different components are present. A small particle of, with a sedimentation coefficient S_{20} that increases steadily to reach a maximum value of about 20 svecbergs, and a heavier component may be distinguished. The lighter component is the amorphous colloid and the heavier one is hematite. In solutions with $\alpha_o > 0.13$ only the heavier, hematite component was observed. The fraction of hematite in the relaxation experiment was also observed to decrease with increasing α_o.

Some of the relaxation curves observed in the pH experiments at 85°C are shown in Figure III.15. A distinctive feature of these curves is the extended plateau-like region at low α_o. The length (in time) of this region decreases with increasing α_o (see Figure III.15b). Again the time, t_i, is located by the inflection point in the

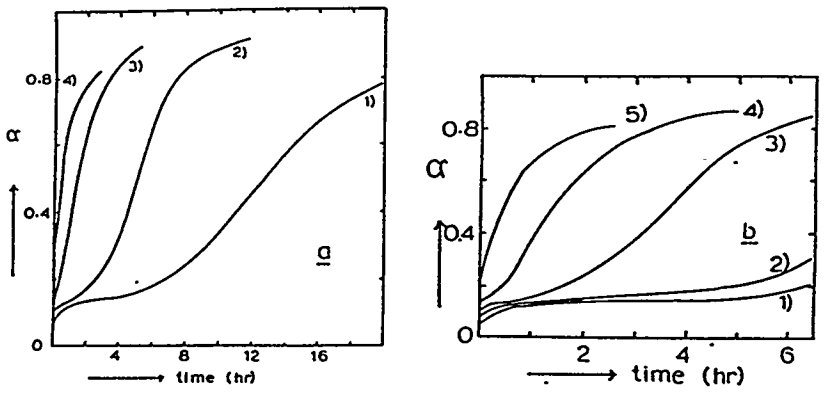

Figure III.15. **(a) Relaxation curves at 85°C. 1. α_o = 0.06, pH 0.86. 2. α_o = 0.09, pH 0.97. 3. α_o = 0.13, pH 1.05. 4. α_o = 0.20, pH 1.16. (b) Enlarged representation of variation of α with t at small values of relaxation time. 1. α_o = 0.06, pH 0.86. 2. α_o = 0.07, pH 0.90. 3. α_o = 0.10, pH 0.99. 4. α_o = 0.13, pH 1.05. 5. α_o = 0.20, pH 1.16 (from reference III.12).**

relaxation curves and is used to characterize the relaxation process at 85°C. Figure III.16 shows an approximately linear relation between log t_i and pH. The slope of the straight line is -10.5.

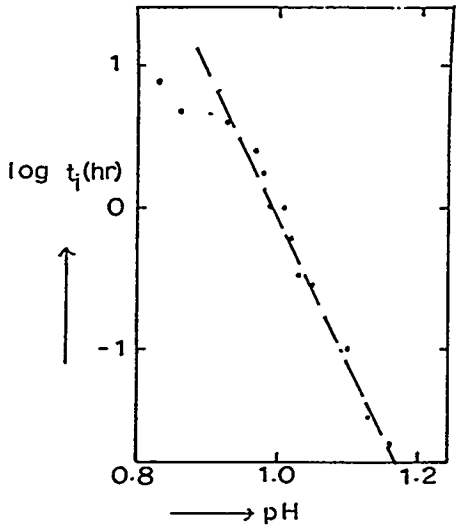

Figure III.16. **The logarithm of the induction time as a function of pH at 85°C. Induction times obtained from Figure III.15 (from reference III.12).**

Figure III.17 presents the authors attempt to indicate the stability regions of the two crystalline phases as a function of temperature (25-100°C) and pH. This diagram was constructed with information obtained by Van der Woude and de Bruyn and from

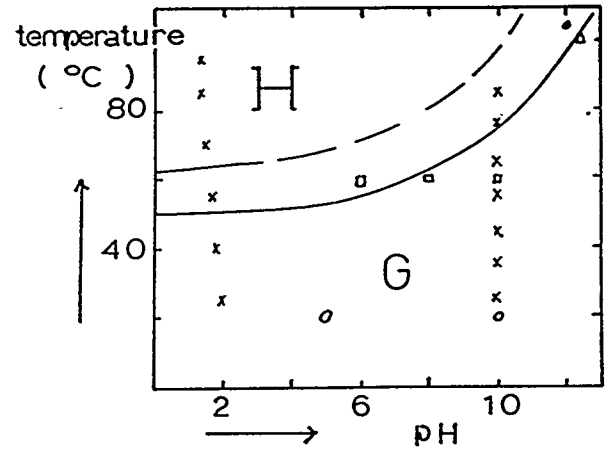

Figure III.17. The stability regions of hematite (H) and geothite (G) as a function of pH and temperature. The width of the region in which phases appear to coexist is outlined with aid of experimental data. X from reference III.11; O from reference III.21; △ from reference III.22; □ from reference III.23; ● from reference III.24 (from reference III.12).

the literature. At low pH, the observed temperature interval over which both crystalline phases may coexist was approximately 10-15°C. The investigation clearly indicated that both geothite and hematite may form via a transformation of the amorphous phase.

Van der Woude and de Bruyn (III.11) also used electron microscopic studies to show the crystalline particles at 25°C and 40°C to have the same length (30 nm) but to vary in width, 4 nm (25°C) and 20 nm (40°C). During aging these particles flocculate into linear arrays with the long dimension of the particles perpendicular to the chain length. This observation corresponds with the findings of Dousma and de Bruyn (III.19). While the aged precipitate at 55°C (a mixture of geothite and hematite) also flocculated, the chain-structure of the sediment so characteristic of the lower